**Electronic Supplementary Information (ESI)**

# Black $BiVO_4$: Size Tailored Synthesis, Rich Oxygen Vacancies, and Sodium Storage Performance

Xiaosa Xu,[#a] Youxun Xu,[#a] Fei Xu,*[ab] Guangshen Jiang,[a] Jie Jian,[a] Huiwu Yu,[a] Enming Zhang,[a] Dmitry Shchukin,[c] Stefan Kaskel[b] and Hongqiang Wang*[a]

[a]State Key Laboratory of Solidification Processing, Center for Nano Energy Materials, School of Materials Science and Engineering, Northwestern Polytechnical University and Shaanxi Joint Laboratory of Graphene (NPU), Xi'an, 710072, P. R. China.

[b]Department of Inorganic Chemistry, Technische Universität Dresden, Bergstrasse 66, 01062 Dresden, Germany.

[c]Department of Chemistry, University of Liverpool, Crown Street, Liverpool L69 7ZD, U.K.

E-mail: feixu@nwpu.edu.cn

hongqiang.wang@nwpu.edu.cn

# Experimental methods

**Synthesis of $BiVO_4$ particles.** All reagents were purchased from Sinopharm Chemical Reagent Co. and used as received. The pristine $BiVO_4$ particles were synthesized by a liquid solid reaction according to the literature.[1] The starting materials $K_3V_5O_{14}$ powders were obtained by calcination of $K_2CO_3$ and $V_2O_5$ in stoichiometric ratio in air at 450 °C for 5 h. $BiVO_4$ particles were synthesized simply by stirring 8 mmol of $K_3V_5O_{14}$ and 40 mmol of $Bi(NO_3)_3{\cdot}5H_2O$ in 200 ml of deionized water at 70 °C for 15 h. The obtained $BiVO_4$ particles collected by centrifugation were washed several times with deionized water. An Nd:YAG laser (pulse width 10 ns, repetition rate 30 Hz) was used as the light source for pulsed laser irradiation. To obtain size tailored $BiVO_4$ colloids, 5 mg of pristine $BiVO_4$ particles was first well dispersed in 5 mL of acetone by ultrasonic vibration. The mixture was then irradiated by an unfocused laser beam with different laser fluences (78, 156, 260 mJ/pulse·cm$^2$, third harmonic) for 10 min.

**Synthesis of BVO@rGO composites.** Graphene oxide (GO) sheets were prepared according to the modified Hummers method. First, 40 mg as-prepared GO was dissolved in 100 mL deionized water under ultrasonication for 1 h to obtain an exfoliated GO suspension. Then, 60 mL as-obtained BVO solution was dropped into the GO suspension slowly under drastic magnetic stirring and the stir needed to sustain 4 h to ensure uniformly anchoring of BVO nanocrystals on the GO matrix. Next, acetone was steamed out and excess ascorbic acid was dissolved in the as obtained suspension. The mixture was then kept at 90 °C for 7 h to reduce the GO to rGO, washed with deionized water for several times. Finally, BVO@rGO was obtained after freeze-drying.

**Structural characterization.** The morphological and structural studies of the collected particles were performed using field-emission scanning electron microscope (FESEM, NANOSEM450, FEI) and transmission electron microscopy (TEM Talos F200X FEI). The crystallinity of the samples was investigated using X-ray diffractometer (Shimadzu XRD-7000). The elementary studies of the samples were conducted using XPS (Shimadzu Kratos Axis Supra). The mass content of BVO was determined via a TG/DTA analyzer (METTLER TOLEDO). The structure was characterized by Raman (InVia, Renishaw, excited by a 532 nm He-Ne laser with a laser spot size of 1 μm).

**Electrochemical measurements**. The working electrodes were prepared by mixing the as-prepared materials (70 wt%), conductive carbon black (Super P, 20 wt%), and binder (polyvinylidene difluoride binder, PVDF, 10 wt%) in n-methyl-2-pyrrolidone (NMP). The resultant slurry was pasted on Cu foil and dried in a vacuum oven at 80 °C for 12 h. Electrochemical measurements were carried out in 2032 typed coin cells, which were assembled into a half-battery in an Ar-filled glove box with the concentrations of moisture and oxygen below 0.1 ppm. The mass loading of the materials on individual electrode was about 1.0 ± 0.1 mg cm$^{-2}$. Sodium metal was used as the counter/reference electrode, and 1 M $NaClO_4$ dissolved in ethylene carbonate (EC) and dimethyl carbonate (DMC) (1:1 by volume) with 5% fluoroethylene carbonate (FEC) as the electrolyte. Glass microfiber (Whatman) film was used as the separator. Galvanostatic charge and discharge measurements were carried out using a LAND CT2001A battery testing system (Wuhan, China) within the voltage range of 0.01−3.0 V. The cyclic voltammogram (CV) with a scan rate of 0.1−1.1 mV s$^{-1}$ and electrochemical impedance spectroscopy (EIS) measurements with a frequency range from 100 kHz to 0.01 Hz were conducted on a CHI electrochemical workstation (Shanghai Chenhua). The specific capacity contribution of $BiVO_4$ in the electrode was calculated according to the Eq. S1.[2]

$$Specific\ capacity\ based\ on\ BVO = \frac{Capacity\ of\ BVO@rGO - capacity\ contribution\ of\ rGO}{Weight\ percentage\ of\ BVO} \quad (1)$$

where the capacity contribution of rGO in the composite was calculated by the Eq. S2.

$$Capacity\ contribution\ of\ rGO = Capacity\ of\ rGO \times Weight\ percentage\ of\ rGO \quad (2)$$

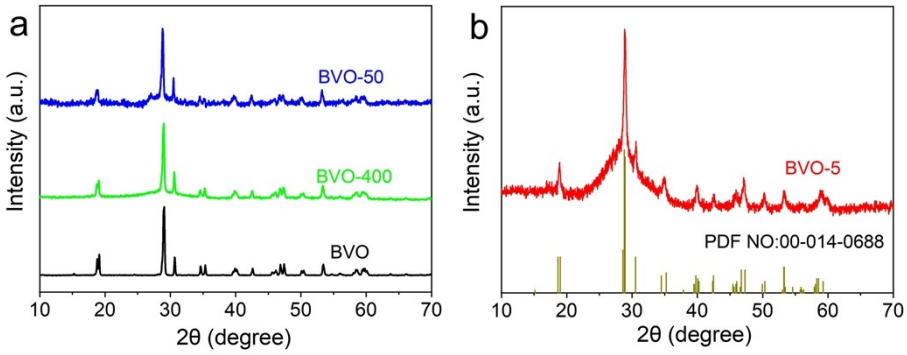


**Fig. S1** (a) XRD patterns of BVO, BVO-400 and BVO-50; (b) XRD pattern of BVO-5.

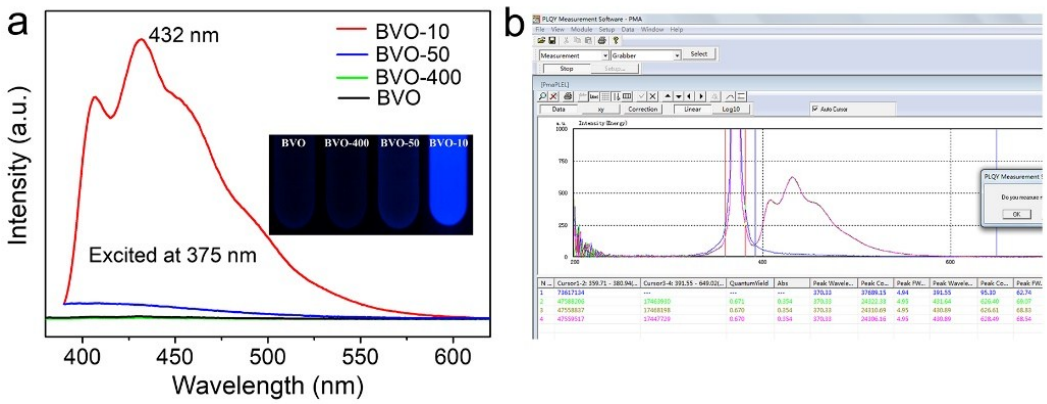


**Fig. S2** (a) Photoluminescence emission spectra of $BiVO_4$ colloidal solution. Insets: photographs $BiVO_4$ dot colloidal solution irradiated by UV light at 365 nm; (b) Absolute photoluminescence quantum yields of BVO-5.

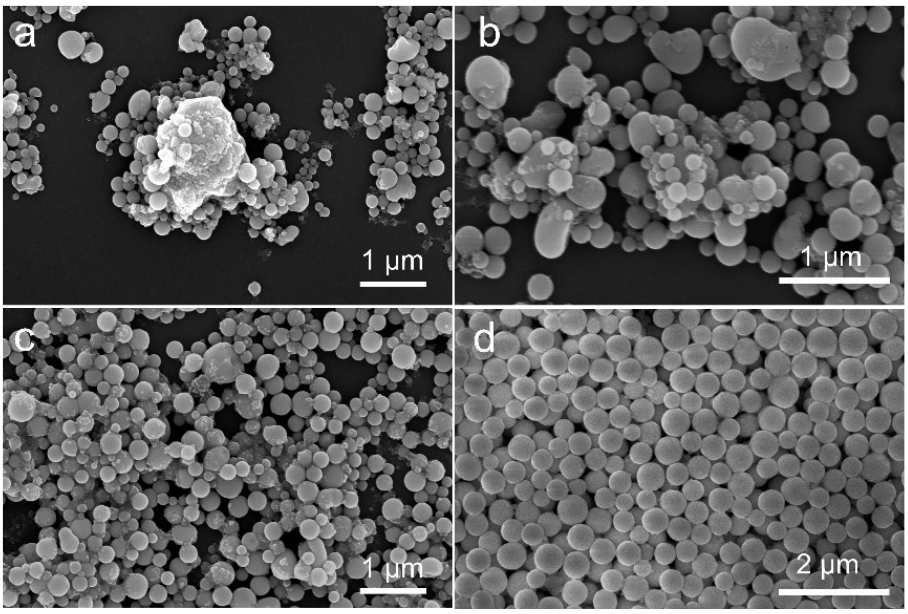


**Fig. S3** SEM images of $BiVO_4$ particles with different laser irradiation period: (a) 30s, (b) 1 min, (c) 5 min and (d) 10 min.

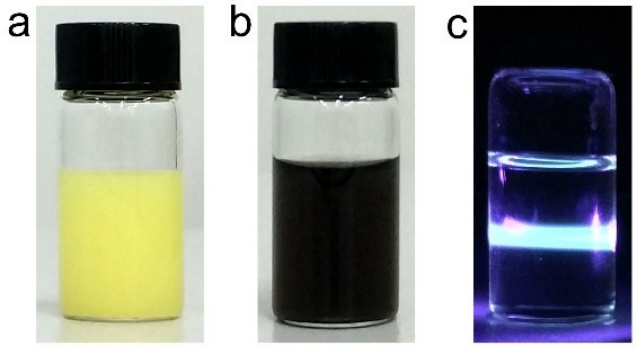


**Fig. S4** (a) Photograph of raw $BiVO_4$ particles dispersed in acetone; (b) Photograph of black $BiVO_4$ colloidal solution after plused laser irradiation; (c) Picture of the scattering of light as a purple light beam passes through the nanocrystals colloid solution.

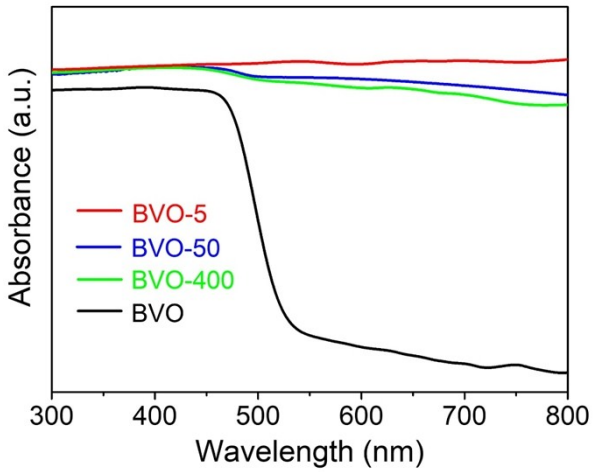


**Fig. S5** UV-vis spectra of BVO, BVO-400, BVO-50 and BVO-5.

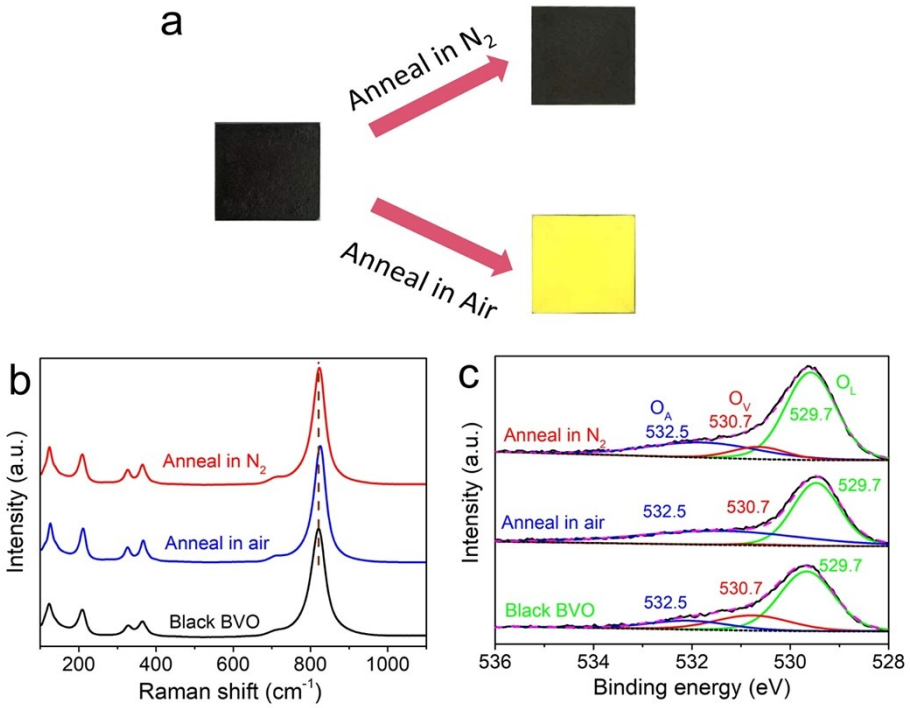


**Fig. S6** (a) Optical images of black $BiVO_4$ dropping onto a glass slide and annealing in air and nitrogen, respectively; (b) Raman spectra and (c) XPS spectra of black $BiVO_4$, annealing in air and annealing in nitrogen.

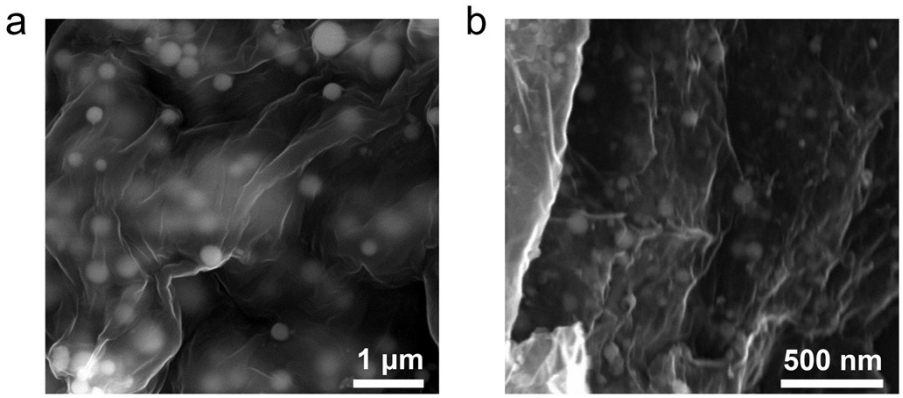


**Fig. S7** (a) SEM image of BVO@rGO-400; (b) SEM image of BVO@rGO-50.

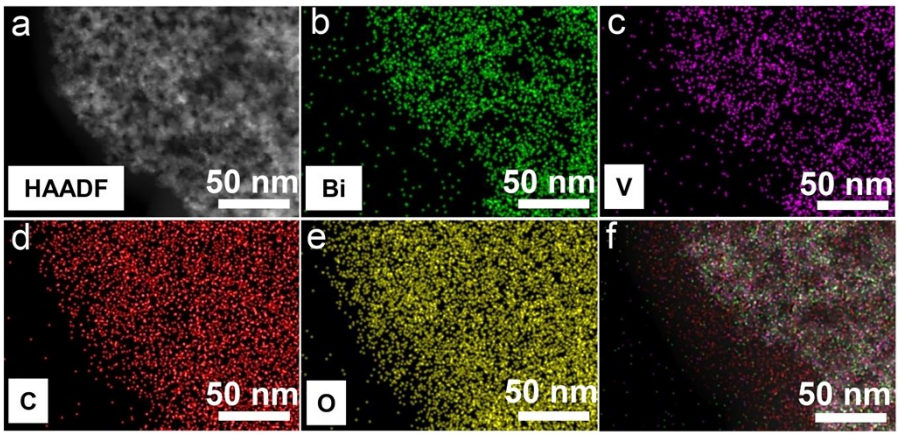


**Fig. S8** (a) Annular dark-field STEM image of BVO@rGO-5; (b–f) Corresponding EDX elemental mapping of bismuth, vanadium, carbon, oxygen, and combinations.

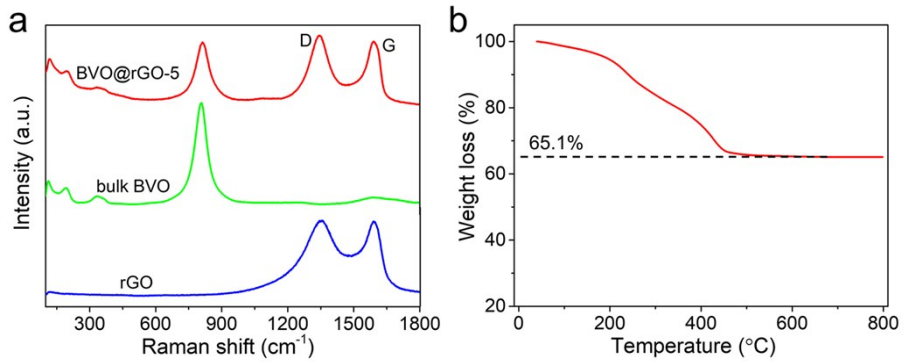


**Fig. S9** (a) Raman spectra of BVO@rGO-5, bulk BVO and rGO; (b) TGA curve of BVO@rGO in air.

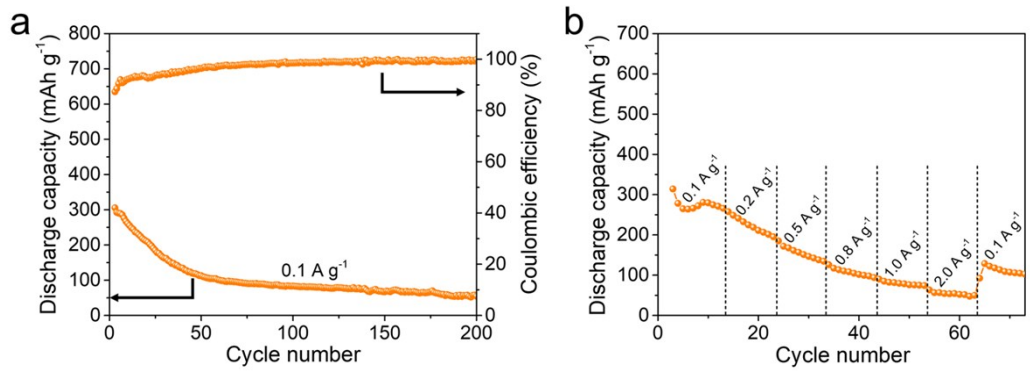


**Fig. S10** (a) Cycling performance of BVO@rGO-*bulk* at 0.1 A $g^{-1}$ within the voltage range of 0.01−3.0 V; (b) Rate capabilities of BVO@rGO-*bulk* electrode from 0.1 to 2.0 A $g^{-1}$.

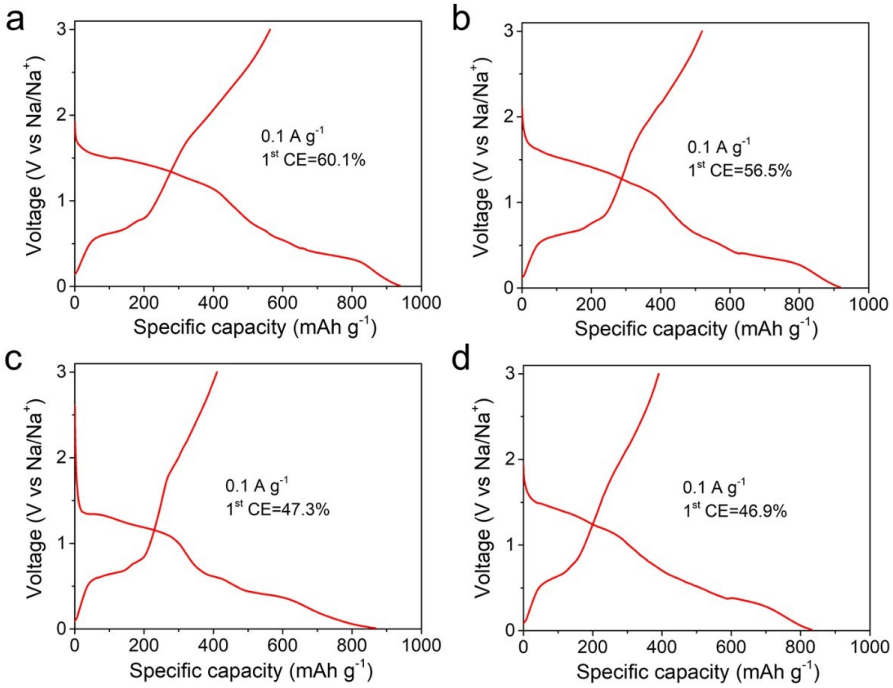


**Fig. S11** The initial discharge and charge voltage profiles of BVO@rGO at 0.1 A $g^{-1}$: (a) BVO@GO-5, (b) BVO@GO-50, (c) *black*-BVO@rGO-400, (d) *yellow*-BVO@rGO-400.

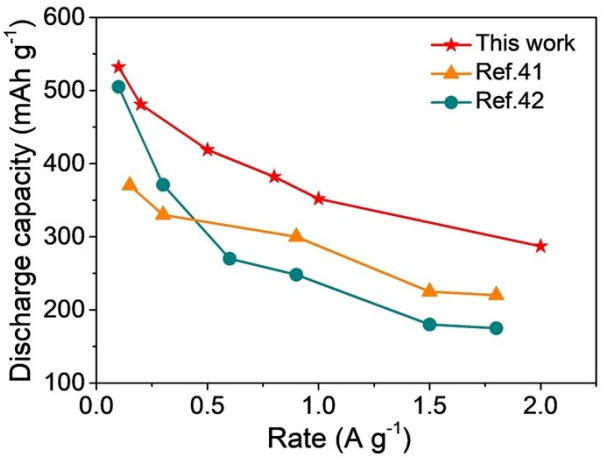


**Fig. S12** Comparison of rate capabilities of the BVO@rGO-5 electrode with BVO-based electrodes in the literature.

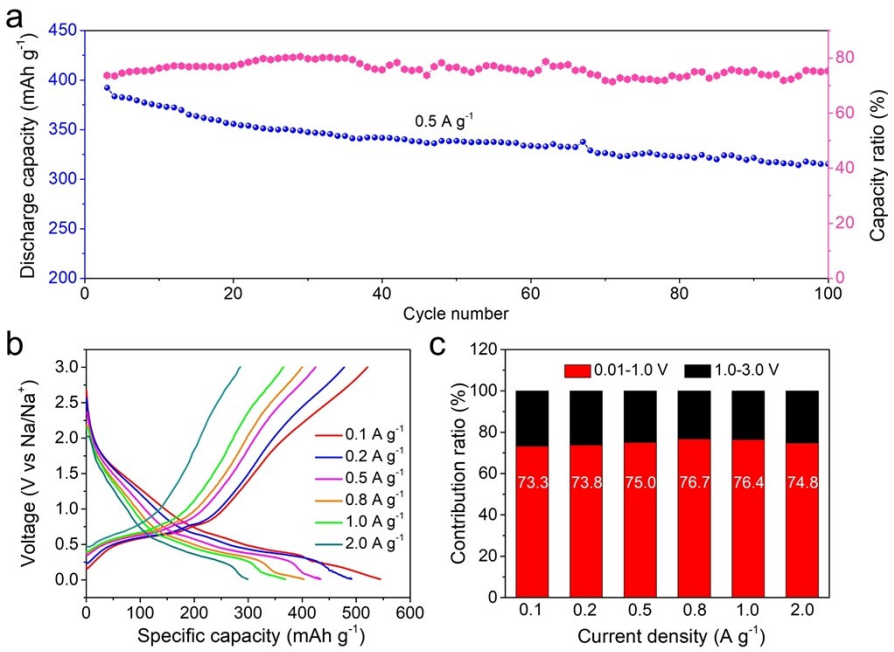


**Fig. S13** (a) Cycling performance of BVO@rGO-5 at 0.5 A $g^{-1}$ with the voltage range of 0.01−1.0 V; (b) Galvanostatic charge-discharge curves of BVO@rGO-5 electrode at different current densities; (c) Capacity proportion of BVO@rGO-5 with the voltage range of 0.01−1.0 V and 1.0−3.0 V at different current densities.

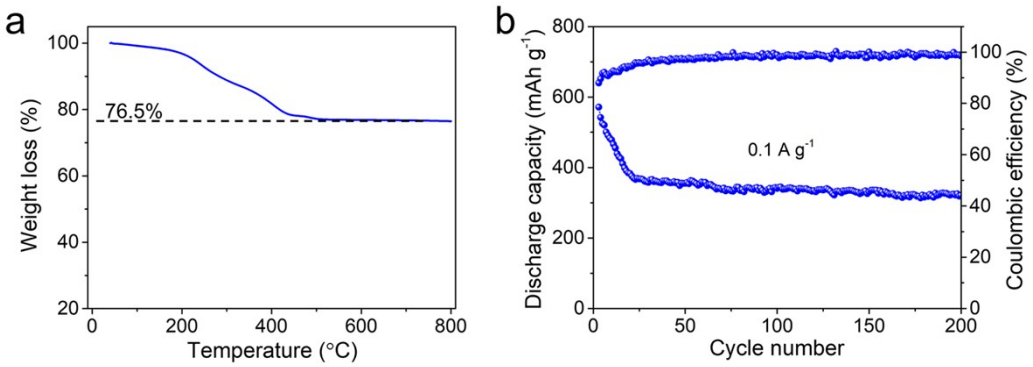


**Fig. S14** (a) TGA curve of BVO@rGO-5-76.5% in air; (b) Cycling performance of BVO@rGO-5-76.5% at 0.1 A $g^{-1}$ within the voltage range of 0.01−3.0 V.

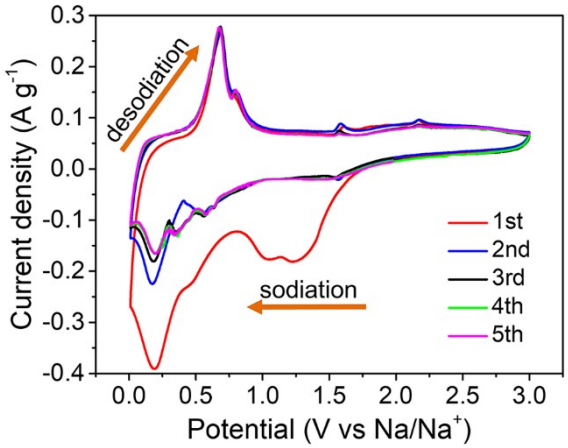


**Fig. S15** First five CV cycles of BVO@rGO-5 electrode at a scan rate of 0.1 mV $s^{-1}$.

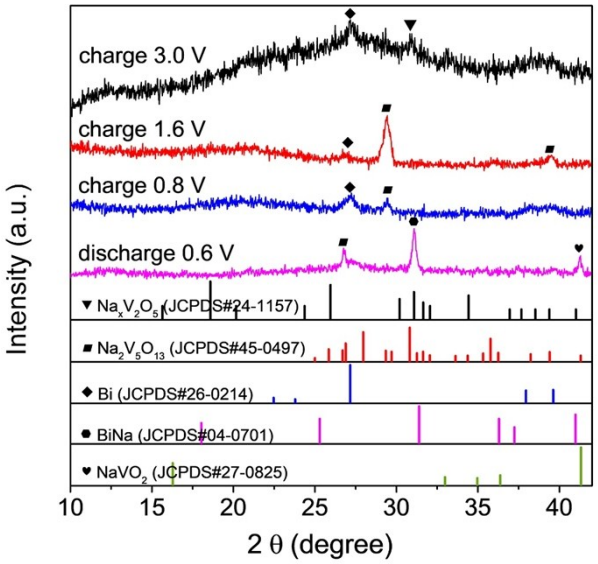


**Fig. S16** Ex-situ XRD patterns of BVO@rGO-5 electrode materials at selected charged/discharged states.

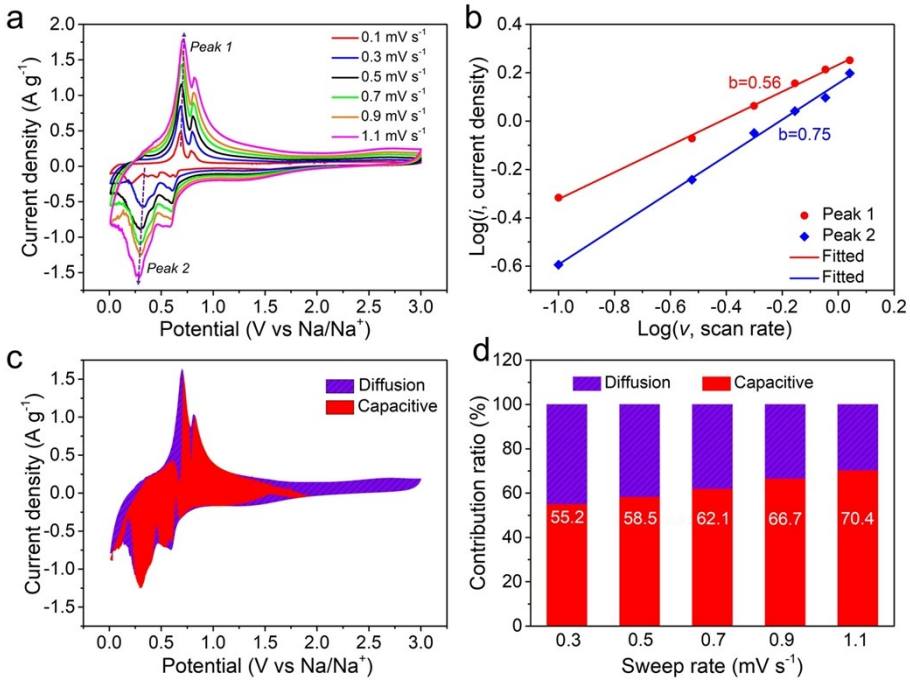


**Fig. S17** (a) CV curves of BVO@rGO-50 electrode at different scan rates; (b) log (*i*) versus log (*v*) plots at different oxidation and reduction states; (c) CV curve with the pseudocapacitive contribution shown in the red region at a scan rate of 0.9 mV $s^{-1}$; (d) The contribution ratio of the capacitive capacity and diffusion-limited capacity at different scan rates in BVO@rGO-50 electrode.

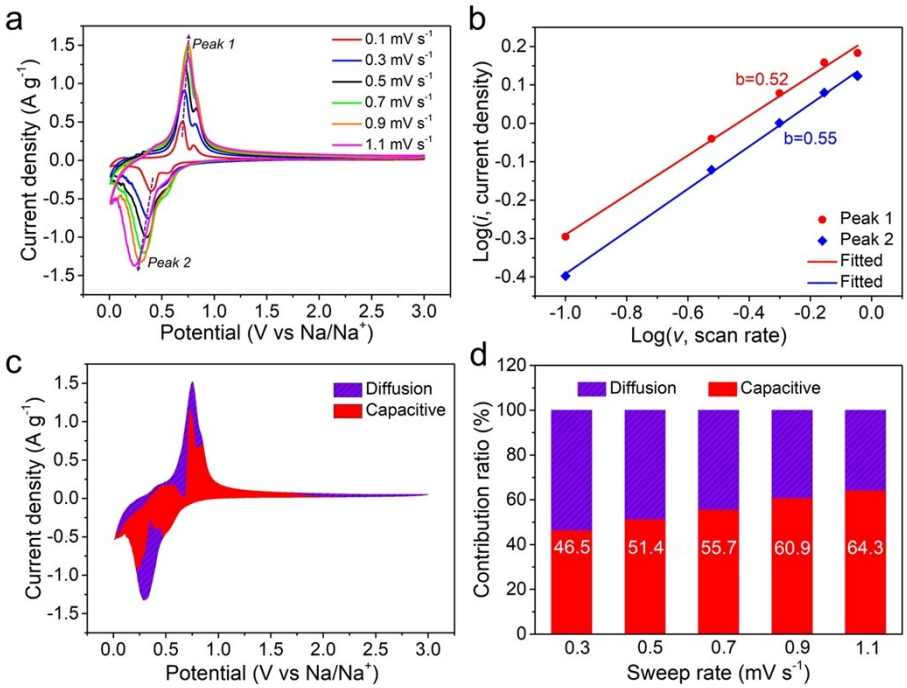


**Fig. S18** (a) CV curves of BVO@rGO-400 electrode at different scan rates; (b) log (*i*) versus log (*v*) plots at different oxidation and reduction states; (c) CV curve with the pseudocapacitive contribution shown in the red region at a scan rate of 0.9 mV $s^{-1}$; (d) The contribution ratio of the capacitive capacity and diffusion-limited capacity at different scan rates in BVO@rGO-400 electrode.

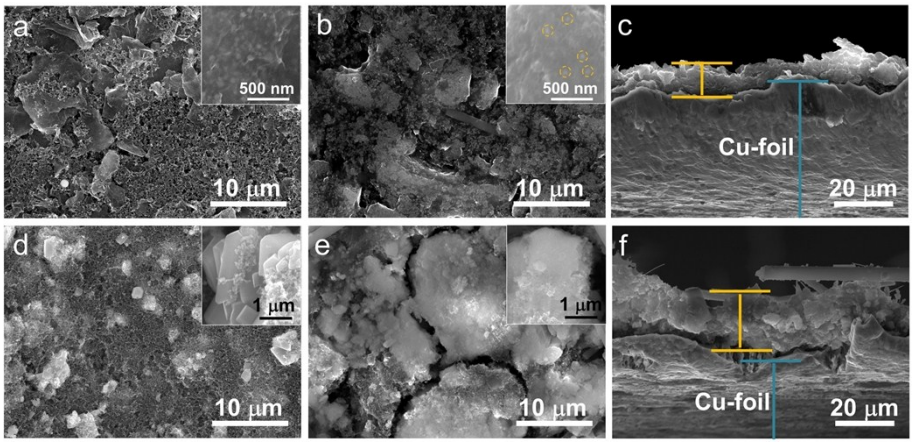


**Fig. S19** (a) Top-view SEM image of fresh BVO@rGO-50 electrode; (b), (c) Top-view and cross-section SEM images of BVO@rGO-50 electrode after 200 cycles, respectively; (d) Top-view SEM image of fresh BVO@rGO-*bulk* electrode; (e), (f) Top-view and cross-section SEM images of BVO@rGO-*bulk* electrode after 200 cycles, respectively. The insets are corresponding images at higher magnification.

**Table S1** Performance records comparisons of different multinary metal oxides based anodes for SIBs.

| Active materials | Cycling stability | | | Rate capability | | References |
|---|---|---|---|---|---|---|
| | Current density [mA $g^{-1}$] | Reversible capacity [mA h $g^{-1}$] | Cycle number | Current density [A $g^{-1}$] | Capacity [mA h $g^{-1}$] | |
| $Ti_2Nb_2O_9$ | 800 | 215 | 500 | 4.0 | 134 | 3 |
| Ni-doped $MnCo_2O_4$ | 100 | 238.6 | 700 | 5.0 | 90 | 4 |
| $CoFe_2O_4$/PPy | 100 | 400 | 200 | 1.0 | 220 | 5 |
| $MnFe_2O_4$/C | 500 | 445 | 300 | 10.0 | 305 | 6 |
| $Na_2Ti_3O_7$ | 177 | 195 | 200 | 6.2 | 65 | 7 |
| $NaTiO_2$ | 29.3 | 152 | 60 | 0.29 | 133.6 | 8 |
| $NaFeTiO_4$/MWCNTs | 8.85 | 160 | 75 | 0.35 | 100 | 9 |
| $Zn_2GeO_4$/C | 100 | 317 | 50 | 2.0 | 150 | 10 |
| $FeCo_2O_4$/Ni-foam | 50 | 422 | 100 | 1.0 | 333 | 11 |
| $NaTi_2(PO_4)_3$/TiN | 266 | 92 | 100 | 1.33 | 57 | 12 |
| $CuFeO_2$ | 100 | 240 | 200 | 1.0 | 63 | 13 |
| $NaTi_2(PO_4)_3$/rGO | 133 | 101 | 200 | 6.65 | 67 | 14 |
| $CoMn_2O_4$/rGO | 200 | 114 | 60 | --- | --- | 15 |
| $NiCo_2O_4$ spheres | 100 | 341 | 100 | 1.0 | 251 | 16 |
| $Sb_2MoO_6$ microspheres | 200 | 637.3 | 100 | 5.0 | 428.1 | 17 |
| $FeTiO_3$/CNTs | 100 | 358.8 | 200 | 5.0 | 201.8 | 18 |
| **$BiVO_4$ nanocrystals/rGO** | **100** | **470** | **200** | **2.0** | **297** | **This work** |

## Supplementary References


1. Y. Kuang, Q. Jia, G. Ma, T. Hisatomi, T. Minegishi, H. Nishiyama, M. Nakabayashi, N. Shibata, T. Yamada, A. Kudo and k. Domen, *Nat. Energy*, 2016, **2**, 16191.
2. W. Li, Z. Yang, M. Li, Y. Jiang, X. Wei, X. Zhong, L. Gu and Y. Yu, *Nano Lett.*, 2016, **16**, 1546.
3. L. Shen, Y. Wang, H. Lv, S. Chen, P. A. Aken, X. Wu, J. Maier and Y. Yu, *Adv. Mater.*, 2018, **30**, 1804378.
4. L. Wu, J. Lang, P. Zhang, X. Zhang, R. Guo and X. Yan, *J. Mater. Chem. A*, 2016, **4**, 18392.
5. Q. He, K. Rui, C. Chen, J. Yang and Z. Wen, *ACS Appl. Mater. Interfaces*, 2017, **9**, 36927.
6. Y. Liu, N. Zhang, C. Yu, L. Jiao and J. Chen, *Nano Lett.*, 2016, **16**, 3321.
7. S. Fu, J. Ni, Y. Xu, Q. Zhang and L. Li, *Nano Lett.*, 2016, **16**, 4544.
8. D. Wu, X. Li, B. Xu, N. Twu, L. Liu and G. Ceder, *Energy Environ. Sci.*, 2015, **8**, 195.
9. X. Hou, C. Li, H. Xu and L. Xu, *Nano Res.*, 2017, **10**, 3585.
10. M. Li, Z. Zhang, X. Ge, Z. Wei, Y. Yao, H. Chen, C. Wang, F. Du and G. Chen, *Chem. Eng. J.*, 2018, **331**, 203.
11. Q. He, S. Gu, T. Wu, S. Zhang, X. Ao, J. Yang and Z. Wen, *Chem. Eng. J.*, 2017, **330**, 764.
12. Z. Liu, Y. An, G. Pang, S. Dong, C. Xu, C. Mi and X. Zhang, *Chem. Eng. J.*, 2018, **353**, 814.
13. D. H. Youn, Y. H. Choi, J. Kim, S. Han, A. Heller and C. B. Mullins, *ChemElectroChem*, 2018, **5**, 2419.
14. C. Wu, P. Kopold, Y. Ding, P. A. Aken, J. Maier and Y. Yu, *ACS Nano*, 2015, **9**, 6610.
15. D. Cai, B. Qu, Q. Li, H. Zhan and T. Wang, *J. Alloys Compd.*, 2017, **716**, 30.
16. X. Zhang, Y. Zhou, B. Luo, H. Zhu, W. Chu and K. Huang, *Nano-Micro Lett.*, 2018, **10**, 13.
17. X. Lu, Z. Wang, K. Liu, J. Luo, P. Wang, C. Niu, H. Wang and W. Li, *Energy Storage Mater.*, 2019, **17**, 101
18. L. Yu, J. Liu, X. Xu, L. Zhang, R. Hu, J. Liu, L. Ouyang, L. Yang and M. Zhu, *ACS Nano*, 2017, **11**, 5120.